Topological quantization of energy transport in micromechanical and nanomechanical lattices

Chih-Chun Chien, Kirill A. Velizhanin, Yonatan Dubi, B. Robert Ilic, and Michael Zwolak

Topological quantization of energy transport in micro- and nano-mechanical lattices

Chih-Chun Chien,[1] Kirill A. Velizhanin,[2] Yonatan Dubi,[3] B. Robert Ilic,[4] and Michael Zwolak[4, *]

[1] School of Natural Sciences, University of California, Merced, CA 95343, USA
[2] Theoretical Division, Los Alamos National Laboratory, Los Alamos, NM 87545, USA
[3] Department of Chemistry and the Ilse Katz Institute for Nanoscale Science and Technology,
Ben-Gurion University of the Negev, Beer-Sheva 84105, Israel
[4] Center for Nanoscale Science and Technology, National Institute of Standards and Technology, Gaithersburg, MD 20899, USA

Topological effects typically discussed in the context of quantum physics are emerging as one of the central paradigms of physics. Here, we demonstrate the role of topology in energy transport through dimerized micro- and nano-mechanical lattices in the classical regime, i.e., essentially "masses and springs". We show that the thermal conductance factorizes into topological and non-topological components. The former takes on three discrete values and arises due to the appearance of edge modes that prevent good contact between the heat reservoirs and the bulk, giving a length-independent reduction of the conductance. In essence, energy input at the boundary mostly stays there, an effect robust against disorder and nonlinearity. These results bridge two seemingly disconnected disciplines of physics, namely topology and thermal transport, and suggest ways to engineer thermal contacts, opening a direction to explore the ramifications of topological properties on nanoscale technology.

Topology gives rise to fascinating phenomena and can lead to the emergence of many exotic states of matter[1–4], from condensed matter[5,6] to cold atoms[7] to quantum computation[8,9]. An example of a lattice with a non-trivial topology is the Su-Schrieffer-Heeger (SSH) model of electrons hopping in polyacetylene[10], which is the focus of many cold-atom studies, e.g., for measuring the Zak phase[11] and demonstrating topological Thouless pumping[12,13]. While there are works focusing on topological effects in the classical regime[14–25], few connect topology and energy transport[26]. We present a mechanical system that manifests topological effects in energy transport and has relevance to many nanoscale scenarios[27,28]. This system is the mechanical counterpart to the SSH model in Fig. 1(a) where alternating nearest neighbor coupling strengths "dimerize" the lattice. When both ends terminate on weak bonds, the whole lattice pairs into dimers. Terminating on a strong bond, though, leaves the end sites unpaired, resulting in the formation of an edge mode. Hence, depending on the topology – e.g., swapping the nearest neighbor couplings constants, which does not change the bulk – there will be zero, one (on either the left or right), or two edge modes.

The mechanical lattice we examine has vibrational spectrum equivalent to the energy spectrum of the SSH model when all parameters (except the alternating nearest-neighbor coupling) are uniform. Otherwise it is identical to the spectrum of a slice of the time-dependent Rice-Mele model, which has a quantized Chern number on the extended 2D plane[4]. The lattice has the Hamiltonian $H = \sum_n \frac{m_n}{2} \left(\dot{x}_n^2 + \omega_n^2 x_n^2 \right) + \sum_n \frac{K_n}{2} (x_n - x_{n+1})^2$ with masses m_n, onsite frequencies ω_n, and nearest-neighbor couplings K_n for site n with coordinate x_n. These parameters, $[m_n, \omega_n, K_n]$, are $[m_1, \omega_1, K_1]$ or $[m_2, \omega_2, K_2]$ for odd or even n, respectively. After a lattice Fourier transform, we get the Bloch Hamiltonian

$$\mathbf{H}_q = h_0 \mathrm{I} + h_z \sigma_z + \bar{\mathbf{H}}_q, \tag{1}$$

where σ_z is the z Pauli matrix, I is the 2×2 identity matrix, and h_z and h_0 are given in the Supplemental Material (SM)[29], and

$$\bar{\mathbf{H}}_q = -\frac{1}{m} \begin{bmatrix} 0 & f^*(q) \\ f(q) & 0 \end{bmatrix}, \tag{2}$$

with $m = \sqrt{m_1 m_2}$ and $f(q) = K_1 + K_2 e^{iq}$. A natural realization of this model is in one-dimensional micro- and nano-electromechanical systems (MEMS-NEMS), which provide a versatile platform for dynamical phenomena and devices[30]. As we will discuss, a combination of laser-induced heating and optical/electronic readout can topologically characterize energy transport in MEMS-NEMS, as shown in Fig. 1(b). However, since this model is one of the most elementary examples of a physical system – classically coupled "masses and springs" – there exists many alternative realizations.

The topological nature of the lattice can be seen by considering $\bar{\mathbf{H}}_q = R_x \sigma_x + R_y \sigma_y$, where $\sigma_{x,y}$ are the Pauli matrices. The curve $(R_x = K_1 + K_2 \cos(q), R_y = -K_2 \sin(q))$ may or may not wrap around the origin in the complex plane as q goes from 0 to 2π. Counting how many times the curve encircles the origin gives the *winding number*,

$$\mathcal{W} = \begin{cases} 1, & K_1 < K_2 \\ 0, & K_1 > K_2 \end{cases}. \tag{3}$$

This number is an important topological property of a 1D system's band structure[1,5]. The Zak phase[31] is the 1D Berry phase and is 2π times the winding number. When the winding number is nonzero, the lattice is topologically non-trivial and edge modes appear, decaying exponentially from the edges with a decay length $\xi = -\log(K_1/K_2)$. Without loss of generality, we use the convention that if only one edge mode is present, it is on the left. The number of left (N_L) and right (N_R) edge modes is thus

$$N_L = \mathcal{W}, \quad N_R = \frac{1 - e^{i\pi(N+\mathcal{W})}}{2}. \tag{4}$$
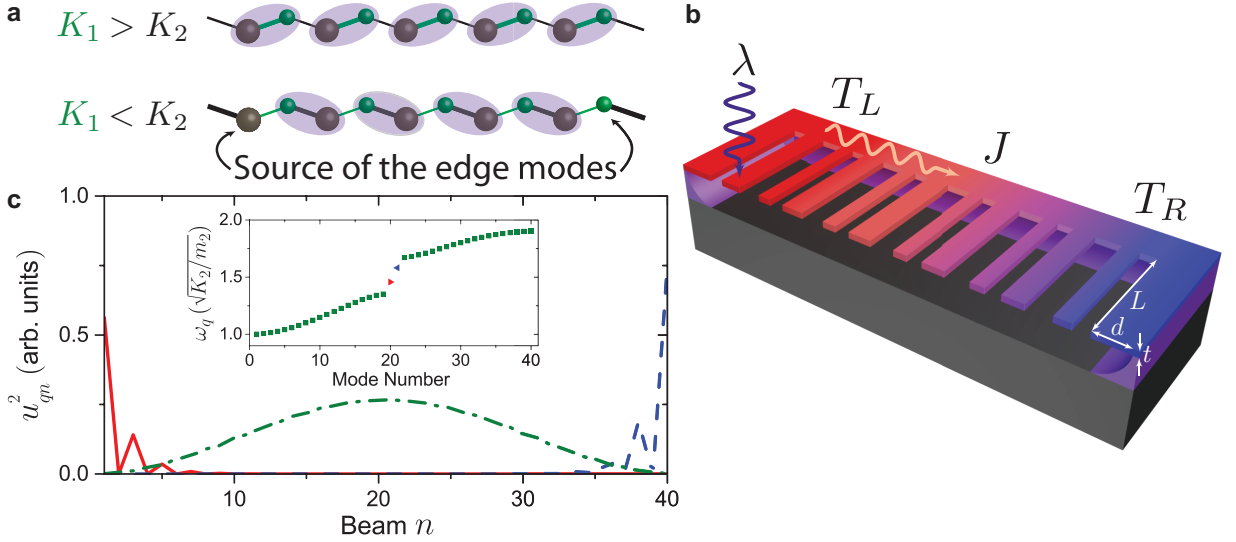
Figure 1. (a) Illustration of dimerization in a mechanically alternating lattice. Intracell (K_1) and intercell (K_2) nearest-neighbor couplings are shown by green and black lines, respectively. Depending on the value of the winding number, Eq. (3), and the parity of the lattice length, N, there can be zero, one, or two edge modes, Eq. (4). For example, when N is even and $K_1 > K_2$ then $\mathcal{W} = 0$ ($K_1 < K_2$ with $\mathcal{W} = 1$) and no edge mode (two edge modes) are present as the strong couplings pair all the sites (all but the two sites at the boundaries) as shown in the left (right) lattice. (b) Illustration of energy transport in an envisioned micro- or nano-mechanical topological lattice. The large and small spacings between beams of length L alternate the nearest neighbor couplings (varying widths can alternate other parameters). Other device characteristics (thickness t, undercut d, device materials) can be used to tune the parameters in Eq. (1). A modulated laser of wavelength λ can equilibrate the end beam of the lattice at some elevated temperature T_L, while the other end is either damped into equilibrium with its surroundings at T_R or its local temperature is measured optically or electronically via its oscillations. A difference in these two temperatures will drive an energy current J. The presence of the edge modes will create an interfacial resistance, as the localized modes tend to decouple the bulk lattice from the boundaries, thereby reducing the ability of energy to flow away from the edge. (c) Three representative normal modes, plotted as the polarization vector squared, u_{qn}^2, versus beam position, n, along the lattice. The two edge modes (solid red and dashed blue lines) are localized around the left and right edges, respectively, while delocalized modes are spread across the entire lattice (dot-dashed green line shows $\sqrt{N}u_{qn}^2$ for one delocalized mode). The parameters are $K_2 = 2K_1$, $m_2 = 3m_1/4$, and $\omega_2 = \omega_1$. The inset shows the frequencies of all modes enumerated in ascending order of frequency. The edge modes reside in the gap between the two bands of delocalized modes.

Figure 1(c) shows the decaying amplitude squared of two edge modes. The σ_z term in Eq. (1), while not present in the SSH model, does not destroy the edge modes as one can verify explicitly (see the SM[29]). Moreover, the edge modes persist in the presence of nonlinearity (see Fig. 2).

These modes are more than just a physical curiosity, however. Figure 1(b) illustrates a lattice of interacting cantilevers with one end at a temperature T_L. When the lattice is locally excited at the boundary, e.g., via a laser as shown in Fig. 1(b), or via an electromagnetic coupling, the resulting energy current will depend on the presence of the edge modes, whether this energy flow is due to a single transient excitation or in a steady-state. The conductance, $\kappa \equiv J/\Delta T$, where ΔT is the temperature difference between two reservoirs, captures this effect. For the bulk, the intrinsic conductance, κ_0, is given by its average phonon group velocity[37]

$$\kappa_0 = \frac{k_B}{2\pi} \int_\Omega dq\, v_q = \frac{k_B \Omega}{2\pi}, \quad (5)$$

where we use Ω to indicate both the bands and the total bandwidth. This is the maximum rate at which a har-monic lattice can transport heat between two equilibrium reservoirs at different temperatures. Since it depends only on the bulk band structure, Ω, it is independent of winding number, i.e., swapping the order of K_1 and K_2 – or changing the parity of the lattice – will not affect it. Reaching this conductance in practice, however, requires that all phonon modes are sufficiently in contact with the reservoirs so that they are supplied ample thermal energy[37]. In the presence of topological edge modes this limit is never reached, and the thermal conductance is always lower than κ_0, regardless of the system length. This is rather surprising, considering the fact that there are at most two edge modes, whereas the number of modes grows linearly with the system size.

We note that the ability of a specific mode q to conduct heat will depend on its contact with the external reservoirs and its intrinsic conductance (determined by its group velocity). In the setup of Fig. 1(b), the strength of the contact of a specific mode q with the reservoirs is given by γu_{q1}^2 and γu_{qN}^2 for the left and right, respectively. The coupling (i.e., damping rate) γ is the strength of contact of the reservoirs to the cantilever beam at the
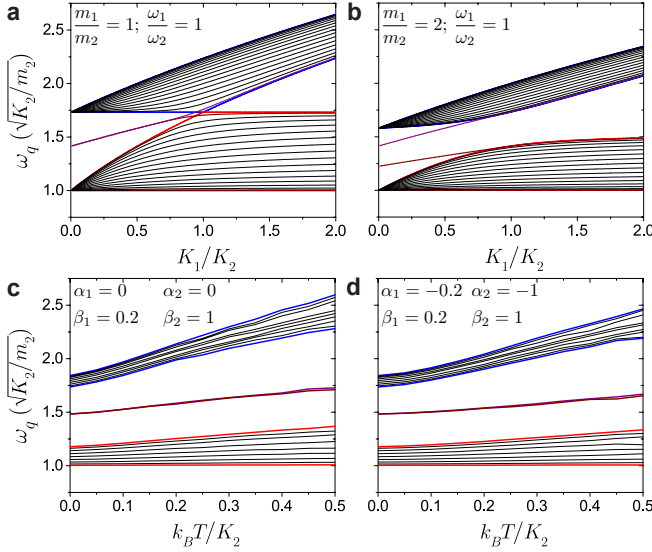
Figure 2. Band structure and edge modes for (a,b) the harmonic lattice (that leads to Eq. (1)) versus the ratio of couplings and (c,d) a nonlinear, FPU-like[32–35] generalization versus temperature. (a,b) When $K_1 < K_2$ in an even site lattice, there are two edge modes (purple and wine lines) that reside in the gap between the two phonon bands (outlined with blue and red for the upper and lower bands, respectively). As K_1 increases the spatial extent of the edge states grows until they merge with the bulk states at $K_1 = K_2$. This process is shown for alternating couplings only (i.e., $m_1/m_2 = 1$; $\omega_1/\omega_2 = 1$) and for the masses alternating (i.e., $m_1/m_2 = 2$; $\omega_1/\omega_2 = 1$). (c,d) The edge modes also exist in nonlinear lattices and persist even as the nonlinearity increases with temperature T (at high enough temperatures, the nonlinearity merges the edge modes with the bulk). The persistence of the edge modes is relevant to MEMS/NEMS, which are often operated in nonlinear regimes[30,36]. Prior studies also show that classical nonlinear systems can exhibit topological excitations[15].

lattice boundary. The polarization vector of the mode on the boundaries, u_{qn}^2 with $n = 1$ or N, attenuates the coupling of the mode q to the reservoirs. When the lattice weakly contacts the reservoirs – in order to minimally perturb the boundaries – the conductance for mode q, κ_q, is due to two contributions in series (see the SM[29])

$$\frac{k_B}{\kappa_q} = \frac{1}{\gamma u_{q1}^2} + \frac{1}{\gamma u_{qN}^2}, \tag{6}$$

where the first term is from the left interface and the second from the right interface. To describe the behavior for arbitrary γ, the bulk contribution – N/v_q, the intrinsic ability of the mode to transfer heat – and an overdamping contribution proportional to γ would need to be included in Eq. (6). Many of the results below hold up to moderate values of γ, as explained in the SM[29].

The edge modes have an exponentially vanishing amplitude, $u_{qn}^2 \approx 0$, for either $n = 1$ or N, which yields $\kappa_q \approx 0$ for $q \in \mathcal{E}$, where $\mathcal{E}$ is the set of edge modes. The

total conductance will then be

$$\kappa = \frac{1}{2\pi} \int_\Omega dq \lim_{N \to \infty} N \kappa_q, \tag{7}$$

where the integral is over only the phonon bands and thus the edge state contribution – which would be a separate sum – is absent. This equation has a similar form to Eq. (5) but κ_q contains the non-ideal contact to the external heat source and sink.

We proceed by giving a heuristic derivation of the effect of topology, and a rigorous derivation is in the SM[29]. Considering all normal modes of a lattice, one has simple "sum rules" for the boundary amplitudes, $\sum_q u_{q1}^2 = 1/m$ and $\sum_q u_{qN}^2 = 1/m$ for the case when $m_1 = m_N = m$, that reflect the (mass) scaling and orthogonal transformations that yield the normal modes. In the absence of edge modes, the bulk modes have a contact strength $u_{qn}^2 \propto \gamma/(mN)$ for $n = 1$ and N. Using this value for u_{qn}^2, the non-topological interfacial conductance for an even length lattice is

$$\bar{\kappa} = \frac{k_B \gamma}{2m}, \tag{8}$$

which is limited by the coupling of the external reservoirs to the lattice, i.e., the heat injected is the bottleneck to current flow[37] (a similar situation occurs in electronic transport[38–40]).

In the presence of edge modes – states localized at the boundaries – the total coupling of the bulk to the reservoirs is reduced: $\sum_{q \in \Omega} u_{qn}^2 = 1/m - \sum_{q \in \mathcal{E}} u_{qn}^2$. The bulk modes therefore have a contact strength $\propto \gamma \left(1 - m \sum_{q \in \mathcal{E}} u_{qn}^2\right)/(mN)$. The amplitude squared of an edge mode on a boundary of its origin is $(1 - e^{-2\xi})/m$, which follows from the normalization of an exponentially decaying state (see the SM[29]). The bulk modes therefore have contact $\gamma u_{qn}^2 \propto \gamma \exp(-2\xi)/(mN)$ for $n = 1$ and N. The conductance in the presence of edge modes is then

$$\kappa = \frac{k_B \gamma e^{-2\xi}}{2m} = e^{-2\xi} \bar{\kappa}. \tag{9}$$

Thus, there is a topologically induced component of the conductance that manifests itself as a prefactor $e^{-2\xi}$.

The case of odd or even N can support $N_L = 0, 1$ states on the left and and $N_R = 0, 1$ states on the right, according to the winding number, Eq. (4). Generalizing Eq. (9) to arbitrary length lattices, and also inhomogeneous mass and on-site frequency cases, the conductance of the lattice is

$$\kappa = \Xi \bar{\kappa}, \tag{10}$$

where $\bar{\kappa}$ is the nontopological component of the conductance (for N odd, $\bar{\kappa} = k_B \gamma/2m_1$; for N even, $\bar{\kappa}$ is the conductance in the absence of edge modes, i.e., K_1 and K_2 swapped, see the SM[29]) and Ξ gives the three discrete

topological levels

$$\Xi = \frac{2}{e^{2N_L\xi} + e^{2N_R\xi}}. \qquad (11)$$

The quantity Ξ is thus a function of winding number, as $N_{L(R)}$ depend on it through Eq. (4). Out of the different configurations (using the parameters that give the same bulk properties but ordering them in different ways), Eq. (11) will give only three possible values, corresponding to the presence of 0,1 or 2 edge modes. All trivial mass effects (at the boundaries) are in $\bar{\kappa}$.

The effect of topological edge modes on thermal conductance is demonstrated in Figure 3, which discusses a uniform lattice with alternating K_1 and K_2 only (solid lines), a lattice with $m_1 = 2m_2$ and $\omega_1 = \omega_2$ (dashed lines) and a lattice with $m_1/m_2 = K_1/K_2$, $\omega_1 = \omega_2$ (dash-dotted lines). For each bulk lattice, we show the case with zero edge modes (green), two edge modes (purple), and one edge mode (red and blue for a left and right edge mode, respectively).

Figure 3(a) plots the thermal conductance κ versus the ratio K_1/K_2. The conductance can take on essentially any value (by changing masses and on-site frequencies, one can fill in the whole plot). However, when taking simple ratios, $\kappa/\bar{\kappa}$, of the thermal conductance, a simple quantization emerges, as shown in Fig. 3(b). These ratios take on just three values given by Ξ. Generically, the introduction of edge modes suppresses the conductance, as it reduces the contact between the energy sources/sinks and the bulk states. Non-topological effects (i.e., the changing bulk state structure as K_1/K_2 increases) can also significantly influence the conductance for certain sets of parameters[41].

Since the suppression of the thermal conductance is a topological effect, it will not depend on the specific details of the system and reservoirs and is anticipated to be robust against various modifications to the lattice (so long as the topology is maintained). We demonstrate this robustness in Fig. 3(c) where we plot the normalized conductance versus K_1/K_2 for three additional lattices; the FPU-β lattice of Fig. 2(c) and two disordered, dimerized lattices. For all these cases, the conductance follows Eq. (10), showing the universality of the

topology-induced reduction of thermal conductance. If the Langevin reservoirs are replaced by uniform harmonic lattices with constant coupling $0 < K < \min(K_1, K_2)$ representing trivial topology, the edge modes and their influence on thermal conductance should still survive at the boundary due to a change of topology.

We further note that Eq. (6) is a general result. It entails, therefore, that even non-topological localized modes (e.g., due to a light mass at the boundary) can suppress the thermal conductance. However, non-topological modes will not display the quantized conductance of Eq. (10) and shown in Fig. 3b,c. As well, there are many channels for heat/energy transport. In the setup envisioned in Fig. 1, heat will also be carried by vibrations of the underlying crystal lattice. Therefore, it is necessary to use a low thermal conductivity material so that vibrations of the cantilevers are the dominant channel for energy transport.

Just as thermal transport can serve as a probe of non-linear structural transitions[42,43], these results show that signatures of nontrivial topologies appear in classical (or quantum) energy transport in conventional physical systems, such as MEMS/NEMS or at crystal-polymer interfaces. In particular, a combination of laser-induced heating and optical/electronic readout will allow for the topological characterization of energy transport in micro- or nano-mechanical lattices and control of heat flow[44]. The emergence of edge states may help design, e.g., thermoelectric devices, where the lattice thermal conductance needs to be suppressed independently of the electronic conductance. Moreover, energy flow and thermal properties are critical to the operation of nanotechnologies, where they can limit and even define the functionality of devices[45–47]. The results presented here thus generate exciting prospects for observing topological properties in conventional physical systems and utilizing them to design micro- and nano-scale devices.

* mpz@nist.gov

[1] M. Z. Hasan and C. L. Kane, Rev. Mod. Phys. **82**, 3045 (2010).

[2] X. L. Qi and S. C. Zhang, Rev. Mod. Phys. **83**, 1057 (2011).

[3] B. A. Bernevig and T. L. Hughes, *Topological insulators and topological superconductors* (Princeton University Press, 2013).

[4] S. Q. Shen, *Topological Insulators: Dirac Equation in Condensed Matters* (Springer-Verlag, 2012).

[5] C. K. Chiu, J. C. Teo, A. P. Schnyder, and S. Ryu, Rev.

Mod. Phys. **88**, 035005 (2016).

[6] A. Bansil, H. Lin, and T. Das, Rev. Mod. Phys. **88**, 021004 (2016).

[7] N. Goldman, J. Budich, and P. Zoller, Nat. Phys. **12**, 639 (2016).

[8] C. Nayak, S. H. Simon, A. Stern, M. Freedman, and S. Das Sarma, Rev. Mod. Phys. **80**, 1083 (2008).

[9] A. Stern and N. H. Lindner, Science **339**, 1179 (2013).

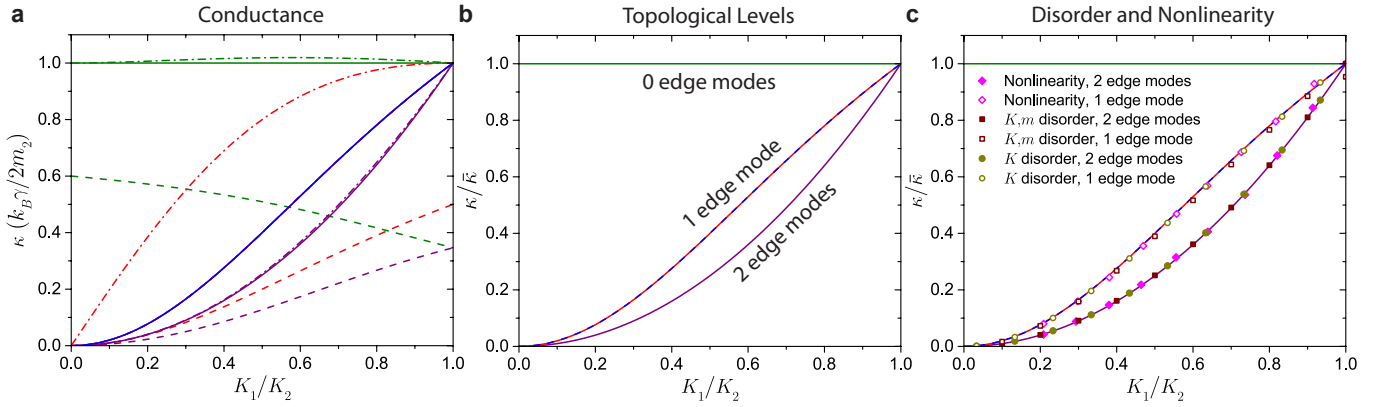[10] W. P. Su, J. R. Schrieffer, and A. J. Heeger, Phys. Rev. Lett. **42**, 1698 (1979).

Figure 3. Topological quantization of the conductance. (a) The conductance versus K_1/K_2 of infinite length dimerized lattices (in the setup shown in Fig. 1(b)). We show only a subset of the curves for clarity, see the SM[29] for details. (b) When taking the ratio of the conductance to the non-topological component, $\bar{\kappa}$, all the curves in (a) collapse onto three distinct levels. Green, purple, and red-blue lines show the cases with zero, two, and one edge mode(s) (left or right), respectively, generically suppressing the conductance. (c) The topological conductance is robust to nonlinearity and disorder. The yellow circles and wine squares show the normalized conductance of two disordered lattices (with both an odd and even number of sites), and the magenta diamonds show the normalized conductances of the FPU lattice. Empty (full) symbols are for one (two) edge modes. Since the nonlinearity also introduces an overall shift in the parameters, the data points are plotted versus an effective K_1/K_2, as described in the SM[29]. In all cases, the results agree with the theoretical result, Eqs. (10) and (11).

[11] M. Atala, M. Aidelsburger, J. T. Barreiro, D. Abanin, T. Kitagawa, E. Demler, and I. Bloch, Nat. Phys. **9**, 795 (2013).
[12] S. Nakajima, T. Tomita, S. Taie, T. Ichinose, H. Ozawa, L. Wang, M. Troyer, and Y. Takahashi, Nat. Phys. **12**, 296 (2016).
[13] M. Lohse, C. Schweizer, O. Zilberberg, M. Aidelsburger, and I. Bloch, Nat. Phys. **12**, 350 (2016).
[14] C. L. Kane and T. C. Lubensky, Nat. Phys. **10**, 39 (2014).
[15] B. G. Chen, N. Upadhyaya, and V. Vitelli, PNAS **111**, 13004 (2014).
[16] R. Susstrunk and S. D. Huber, Science **349**, 47 (2015).
[17] J. Paulose, B. G.-g. Chen, and V. Vitelli, Nat. Phys. **11**, 153 (2015).
[18] S. D. Huber, Nat. Phys. **12**, 621 (2016).
[19] L. Lu, J. D. Joannopoulos, and M. Soljacic, Nat. Photonics **8**, 821 (2014).
[20] N. Berg, K. Joel, M. Koolyk, and E. Prodan, Phys. Rev. E **83**, 021913 (2011).
[21] Z. Yang, F. Gao, X. Shi, X. Lin, Z. Gao, Y. Chong, and B. Zhang, Phys. Rev. Lett. **114**, 114301 (2015).
[22] I. Kim, S. Iwamoto, and Y. Arakawa, Appl. Phys. Express **11**, 017201 (2018).
[23] P. Wang, L. Lu, and K. Bertoldi, Phys. Rev. Lett. **115**, 104302 (2015).
[24] A. B. Khanikaev, R. Fleury, S. H. Mousavi, and A. Alu, Nat. Comm. **6**, 8260 (2015).
[25] Z. Y. Ong and C. H. Lee, Phys. Rev. B **94**, 134203 (2016).
[26] A. Bid, N. Ofek, H. Inoue, M. Heiblum, C. L. Kane, V. Umansky, and D. Mahalu, Nature **466**, 585 (2010).
[27] A. Dhar, Adv. Phys. **57**, 457 (2008).
[28] Z. Xu, Theor. Appl. Mech. Lett. **6**, 113 (2016).
[29] See Supplemental Material at [URL will be inserted by publisher. [The pdf file contains the details of this work.]].
[30] M. Sato, B. E. Hubbard, and A. J. Sievers, Rev. Mod. Phys. **78**, 137 (2006).
[31] J. Zak, Phys. Rev. Lett. **62**, 2747 (1989).
[32] V. Burkalov, S. Kiselev, and V. Pyrkov, Solid State Commun. **74**, 327 (1990).
[33] G. James and M. Kastner, Nonlinearity **20**, 631 (2007).
[34] R. Livi, M. Spicci, and R. S. MacKay, Nonlinearity **10**, 1421 (1997).
[35] M. Aoki, J. Phys. Soc. Jpn. **61**, 3024 (1992).
[36] M. Sato, B. E. Hubbard, A. J. Sievers, B. Ilic, D. A. Czaplewski, and H. G. Craighead, Phys. Rev. Lett. **90**, 044102 (2003).
[37] K. A. Velizhanin, S. Subin, C.-C. Chien, Y. Dubi, and M. Zwolak, Sci. Rep. **5**, 17506 (2015).
[38] D. Gruss, K. Velizhanin, and M. Zwolak, Sci. Rep. **6**, 24514 (2016).
[39] J. E. Elenewski, D. Gruss, and M. Zwolak, J. Chem. Phys. **147**, 151101 (2017).
[40] D. Gruss, A. Smolyanitsky, and M. Zwolak, J. Chem. Phys. **147**, 141102 (2017).
[41] C. C. Chien, S. Kouachi, K. A. Velizhanin, Y. Dubi, and M. Zwolak, Phys. Rev. E **95**, 012137 (2017).
[42] K. A. Velizhanin, C. C. Chien, Y. Dubi, and M. Zwolak, Phys. Rev. E **83**, 050906(R) (2011).
[43] C. C. Chien, K. A. Velizhanin, Y. Dubi, and M. Zwolak, Nanotech. **24**, 095704 (2013).
[44] N. Li, J. Ren, L. Wang, G. Zhang, P. Hänggi, and B. Li, Rev. Mod. Phys. **84**, 1045 (2012).
[45] Y. Dubi and M. Di Ventra, Rev. Mod. Phys. **83**, 131 (2011).
[46] N. Li, J. Ren, L. Wang, G. Zhang, P. Hänggi, and B. Li, Rev. Mod. Phys. **84**, 1045 (2012).
[47] N. Yang, X. Xu, G. Zhang, and B. Li, AIP Adv. **2**, 041410 (2012).